

Observational Evidence For Constant Gas Accretion Rate Since $z = 5$

Eleanor F. Spring¹ and Michał J. Michałowski^{1,2}

¹*Institute for Astronomy, University of Edinburgh, Royal Observatory, Blackford Hill, Edinburgh EH9 3HJ, UK*

²*Astronomical Observatory Institute, Faculty of Physics, Adam Mickiewicz University, ul. Słoneczna 36, 60-286 Poznań, Poland*

Accepted XXX. Received YYY; in original form ZZZ

ABSTRACT

Star formation rate density (SFRD) has not been constant throughout the history of the Universe. The rate at which stars form greatly affects the evolution of the Universe, but the factors which drive SFRD evolution remain uncertain. There must be sufficient amount of gas to fuel the star formation, either as a reservoir within a galaxy, or as inflow from the intergalactic medium (IGM). This work explores how the gas accretion rate onto galaxies over time has affected star formation rate. We propose a novel method of measuring cosmic gas accretion rate. This involves comparing the comoving densities of available HI and H₂ gas and the densities of existing stars at different redshifts. We constrained gas accretion until $z = 5$, and we found that the gas accretion rate density (GARD) is relatively constant in the range from $z = 5$ to $z = 0$. This constancy in the GARD is not reflected by the SFRD, which declines significantly between $z = 1.0$ and $z = 0$. This work suggests that the decline is not due to a reduction in GARD.

Key words: galaxies: evolution, intergalactic medium, galaxies: ISM, galaxies: star formation

1 INTRODUCTION

One of the most important issues of the evolution of the Universe is how galaxies acquire gas which fuels star formation. Numerical galaxy formation models require significant gas inflows from the intergalactic medium (IGM) to fuel star formation (Dekel & Birnboim 2006; Dekel et al. 2009; Schaye et al. 2010), and indeed the current gas reservoirs in many galaxies are too low to sustain the current level of star formation, even for normal galaxies like the Milky Way (Draine 2009). This is reinforced by simulations of l’Huillier et al. (2012), who found that most galaxies assemble their mass through steady gas accretion, and only most massive galaxies grow predominately due to dramatic merger events. However, such inflow process cannot be studied in details because it is very difficult to directly detect it. Only for a few galaxies was the observational indication of gas inflow obtained (Martin et al. 2014; Turner et al. 2015; Rauch et al. 2016), and indirect evidence was reviewed by Sancisi et al. (2008).

Michałowski et al. (2015, 2016) provide evidence for gas inflow directly fueling star formation. This was achieved by reporting the first 21 cm line observations for long gamma-ray burst galaxies. These observations implied high levels of HI gas in areas of recent star formation, whereas low molec-

ular gas content was reported for GRB hosts (Hatsukade et al. 2014; Stanway et al. 2015; Michałowski et al. 2016, but see Perley et al. 2017). This in turn suggests that star formation is either directly fueled by HI gas, or that there is a very efficient conversion process between HI and H₂ under-way (Michałowski et al. 2015).

As reported by Sancisi et al. (2008) within the Milky Way itself, rate of star formation has been very constant over the course of its life. This clearly demonstrates that the gas being used up in star formation is somehow being replaced. Whilst it is obvious that gas accretion must be happening for almost all galaxies, it is very unclear how much is taking place.

Whilst there is a wide range of theories regarding the evolution of star formation rate, there is little observation based evidence available to study the details of this process. Observations suggest that it is the accretion of metal-poor gas that drives the formation of disc galaxies (Sanchez-Almeida et al. 2014, 2013; Cresci et al. 2010). There has been a lot of work done to measure the densities of HI and H₂ mass in galaxies at varying redshifts. In order to detect H₂ gas, the CO molecule is generally used as a tracer (Carilli & Water 2013; Bolatto et al. 2013).

The aim of this paper is to provide the first observational measurement of the cosmic gas accretion rate density (GARD) by applying a novel method, and comparing it to

* E-mail: eleanorspring@hotmail.co.uk

the measurement of the star formation rate density (SFRD). A cosmological model with $h = 0.7$, $\Omega_m = 0.3$, $\Omega_\Lambda = 0.7$ is assumed.

2 DATA

The compilations of ρ_{HI} and ρ_{H_2} from [Lagos et al. \(2014\)](#) and [Hoppmann et al. \(2015\)](#) were used. Significantly more ρ_{HI} data was available than ρ_{H_2} , over a wider redshift range. We used the compilation of $\rho_{stellar}$ (including stellar remnants) from [Michalowski et al. \(2010\)](#).

The HI densities were obtained by a variety of methods over the redshift range. These included spectral stacking of the 21-cm Hydrogen emission line and damped Lyman- α (DLA) absorbers. The complete compilation of ρ_{HI} measurements is presented in table B1. All density values are densities per unit of comoving volume.

The values from [Zwaan et al. \(2005\)](#) and [Martin et al. \(2010\)](#) were for the local universe, at $z = 0$. The [Martin et al. \(2010\)](#) value was based on the Arecibo Legacy Fast ALFA (ALFALFA) survey, which at that time had completed source extraction for 40% of the total sky area, allowing the value to be calculated from a sample of 10 119 galaxies. In comparison, the [Zwaan et al. \(2005\)](#) value was based on the HI Parkes All Sky Survey (HIPASS) which was based on 4315 extra galactic emission-line detections. As such, it was reasonable to assume that the [Martin et al. \(2010\)](#) value is superior to the [Zwaan et al. \(2005\)](#) value. The [Freudling et al. \(2011\)](#) value was given relative to $z = 0$, so required a conversion using an established value of ρ_{HI} at $z = 0$. The [Lah et al. \(2007\)](#) was based on observations from the Giant Metrewave Radio Telescope (GMRT) in order to measure ρ_{HI} at $z = 0.24$. The [Delhaize et al. \(2013\)](#) values were based on a combination of detected sources and the spectral stacking technique. Contrary to previous estimates, they also suggested that ρ_{HI} evolution over the last 1 Gyr was minimal. The [Rhee et al. \(2013\)](#) values were obtained using HI signal stacking technique. The [Hoppmann et al. \(2015\)](#) values also relied upon the detection of hydrogen 21-cm emission with Arecibo Ultra Deep Survey.

[Chang et al. \(2010\)](#) used the HI intensity mapping based on the DEEP2 optical galaxy redshift survey. The [Masui et al. \(2013\)](#) value was obtained by cross-correlating hydrogen 21-cm information with data from the WiggleZ Dark Energy Survey.

The [Péroux et al. \(2003\)](#), [Rao et al. \(2006\)](#), [Noterdaeme et al. \(2012\)](#), [Zafar et al. \(2013\)](#), and [Prochaska & Wolfe \(2009\)](#) values were all obtained using data from surveys of damped Lyman- α (DLA) absorbers.

The ρ_{H_2} values were sourced from [Kereš et al. \(2003\)](#) for $z = 0$, and [Decarli et al. \(2016\)](#) for other redshifts.

3 METHOD: GAS ACCRETION RATE DENSITY (GARD) ESTIMATE

In the calculations presented below care must be taken in consistently treating the extent of the gas and stellar components which are considered to lie inside or outside a galaxy. Here we broadly define a galaxy extent as the size of the atomic gas disk, which is usually a few times larger than the

stellar disk, i.e. extends for a few tens of kpc. In this definition the hot gas in the dark matter halo is not considered.

Absorption measurements of ρ_{HI} in principle could trace the gas outside galaxies, but the DLA systems used for these studies are dense enough to safely assume that they are associated with galaxies. Indeed, DLAs have SFRs and velocity dispersions characteristic for galaxies, and metallicities higher than that of the IGM (e.g. [Møller et al. 2004](#); [Wolfe et al. 2005](#); [Ledoux et al. 2006](#); [Fynbo et al. 2010, 2011, 2013](#); [Krogager et al. 2012, 2013](#)). Moreover within the error bars there is no step change from HI-line- to DLA-derived ρ_{HI} values (Fig. A1 and Table B1), which would be expected if DLAs probed additional neutral gas component in the IGM. Finally, the sizes of the absorbing gas of DLAs are ~ 10 – 20 kpc ([Møller et al. 2004](#); [Péroux et al. 2005](#); [Wolfe et al. 2005](#); [Monier et al. 2009](#); [Fynbo et al. 2010, 2011, 2013](#); [Krogager et al. 2012, 2013](#)), safely within our limit of a few tens of kpc. There are some known DLAs with impact parameters from the background quasar of 50–100 kpc (right part of Fig. 18 in [Rao et al. 2011](#)), but these DLAs are rare (three out of 27 DLAs in the sample of [Rao et al. 2011](#)), so their impact on the measured ρ_{HI} is minor. Moreover, they all have low identification confidence. Similarly, simulations show that the hydrogen density required to classify as a DLA ($2 \times 10^{20} \text{ cm}^{-2}$; [Wolfe et al. 2005](#)) is only present within ~ 20 kpc from the galaxy centre ([Liang et al. 2016](#) fig. 7 and 18; [Shen et al.](#), in prep.).

Calculating the GARD involves the following steps. The total matter density inside galaxies for each redshift bin was calculated as:

$$\rho_{total} = \rho_{HI} + \rho_{H_2} + \rho_{stel}. \quad (1)$$

Over time this density changes only by inflows and outflows:

$$\rho_a = \rho_b + \rho_{inflow} - \rho_{outflow} \quad (2)$$

Where a and b represent total ρ at different epochs. We do not distinguish different mechanisms of inflow and outflow, so these terms include all processes that add to and remove gas from galaxies, respectively. The inflow processes include cold and hot mode accretion, as long as the gas ends up inside galaxies (as defined above) during the relevant time span. It also includes gas expelled to the galactic halo during star-formation episodes which is subsequently re-accreted. Galactic fountains eject cold high-metallicity gas into the corona, and by mixing, cool the low-metallicity gas of the corona sufficiently that fountain clouds form and inflow back into the galactic disc ([Fraternali. 2014](#)). Gas accreted from fountain clouds is considered inflow. Accretion of gas into intra-cluster medium is not included, as such gas does not end up inside galaxies, and is not included in the HI and H_2 measurements. The outflows include supernova and AGN feedback, gas stripping, etc.

The average density of gas accreted by galaxies between two epochs (i.e. the difference between the gas flowing in and out) can be calculated as:

$$\text{GAD} \equiv \rho_{inflow} - \rho_{outflow} = \rho_a - \rho_b \quad (3)$$

By calculating the *difference* in ρ_{total} between consecutive epochs, represented in equation 3 by ρ_a and ρ_b , only the

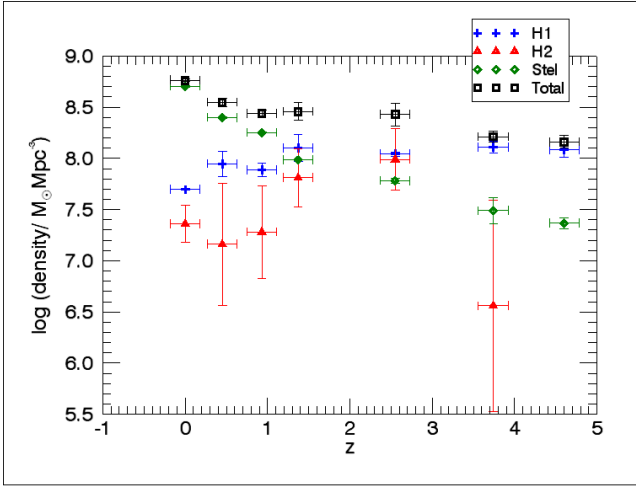


Figure 1. The gas and stellar mass densities per unit of comoving volume : ρ_{HI} (blue crosses); ρ_{H_2} (red triangles); ρ_{stel} (green diamonds); total ρ , a summation of the three contributors (black squares), against redshift, z . The z ‘error’ indicates bin width.

gas remaining within the galaxy — either free or as stars — is accounted for. This quantity was labelled the gas accretion density (GAD). From there, the GARD could then be calculated using:

$$\text{GARD} = \frac{\text{GAD}}{\Delta\text{time}}. \quad (4)$$

Where Δtime was the time elapsed between neighboring redshift bins.

4 RESULTS

The binned values for all three data sets are presented in Table 1 and can be seen in Figure 1 extending between $z = 0$ to $z = 5$. The first six bins cover points where ρ_{HI} , ρ_{H_2} and ρ_{stel} data were all available. The seventh and final bin centred at $z = 4.6$ does not include ρ_{H_2} data, as none was available at that redshift. It seemed legitimate to continue to seven bins, as the contribution to ρ_{tot} from ρ_{H_2} was already very minimal in the sixth bin, relative to those of ρ_{HI} and ρ_{stel} . There is a clearly decreasing trend in ρ_{tot} . This is primarily due to the ρ_{stel} data dominating at $z < 2$.

Both GAD and GARD are presented in Table 2. The value of GAD (see Equation 3) represents the density present at a lower redshift that had not been present previously, either as a fresh gas reservoir or newly formed star. For plots of GAD against redshift, z see Appendix A. Figure 2 compares the GARD with SFRD. It can be seen that the GARD values seem to be relatively constant. This does not tally with the clear drop in SFRD observed from between $z = 1.5$ to 0.

The errors in GAD and GARD were calculated by propagating the errors of individual densities in a standard manner, whereas the errors of these densities are the errors of the means of the densities in relevant redshift ranges reported in other studies.

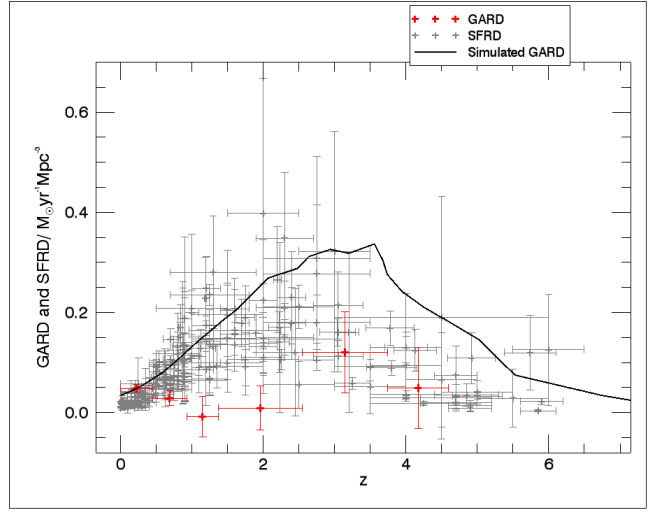


Figure 2. SFRD (grey crosses) using a compilation from Michałowski et al. (2010), the GARD (this work, red symbols), and the simulated GARD for smooth gas accretion (fig. 12 of Kereš et al. 2005). Due to a slight increase in ρ_{tot} between the bins centred at $z = 1.37$ and 0.93 in an otherwise downward trend (see Table 1) the GAD value — and therefore the GARD value — spanning these bins is negative. For the GAD values, see Table 2.

Table 1. Binned comoving gas and stellar mass densities.

z	$\log(\rho_{HI})$ [$M_{\odot}Mpc^{-3}$]	$\log(\rho_{H_2})$ [$M_{\odot}Mpc^{-3}$]	$\log(\rho_{stel})$ [$M_{\odot}Mpc^{-3}$]	$\log(\rho_{tot})$ [$M_{\odot}Mpc^{-3}$]
0.0	7.70 ± 0.01	7.36 ± 0.18	8.70 ± 0.01	8.76 ± 0.01
0.45	7.95 ± 0.12	7.16 ± 0.60	8.40 ± 0.01	8.55 ± 0.04
0.93	7.89 ± 0.06	7.28 ± 0.45	8.25 ± 0.01	8.44 ± 0.04
1.37	8.10 ± 0.13	7.81 ± 0.28	7.98 ± 0.01	8.46 ± 0.09
2.55	8.04 ± 0.02	7.99 ± 0.30	7.78 ± 0.03	8.43 ± 0.12
3.74	8.11 ± 0.06	6.56 ± 1.03	7.49 ± 0.13	8.21 ± 0.06
4.60	8.09 ± 0.07	—	7.37 ± 0.05	8.16 ± 0.06

Table 2. Gas accretion density (GAD) and gas accretion rate density (GARD). The time spanned by each of the redshift bins is included under Δtime .

z	Δtime [Gyr]	GAD [$10^7 M_{\odot}Mpc^{-3}$]	GARD [$10^{-2} M_{\odot}yr^{-1}Mpc^{-3}$]
0.45 - 0.0	4.76	22.59 ± 3.51	4.83 ± 0.75
0.93 - 0.45	2.75	7.88 ± 3.96	2.86 ± 1.44
1.37 - 0.93	1.51	-1.25 ± 6.07	-0.83 ± 4.03
2.55 - 1.37	2.01	1.81 ± 8.81	0.90 ± 4.38
3.74 - 2.55	0.88	10.56 ± 7.11	12.02 ± 8.09
4.60 - 3.74	0.36	1.78 ± 2.91	4.92 ± 8.06

5 DISCUSSION

We did not find significant variations in GARD. Indeed, a straight line fit to the GARD vs. redshift plot resulted in a slope of $-0.009 \pm 0.013 M_{\odot}yr^{-1}Mpc^{-3}$, consistent with no evolution. However, argument could be made for an increasing trend in GARD from $z = 2$ to the present. This is an unex-

pected result as it does not tally up with the SFRD which increases relatively steadily from $z = 5$ to $z = 1.5$, and then declines from around $z = 1.5$ to $z = 0$. Therefore, the decline in SFRD observed cannot be attributed to a change in gas accretion rate. It seems that galaxies in the earlier universe used up their gas supplies faster than the accretion of fresh gas could maintain (SFRD > GARD). SFRD now has dropped beneath the GARD, so the current SFRD is now sustainable. This drop in SFRD is therefore not due to decrease in gas supply. It could be because average density of gas in galaxies dropped, leaving significant amounts of gas below the star-formation threshold.

In order to compare our unexpected results with those from a well established simulation Figure 2 compares GARD from this work with that obtained from a smoothed particle hydrodynamics simulation including dark matter, gas, and stars from Kereš et al. (2005). Simulated GARD shows a distinctive decline from $z < 4$ which more closely echoes SFRD than the GARD from this work, however, there is a convincing order of magnitude consistency between the values. There are a few feasible explanations for the discrepancies between the simulation and the results from this work. It is possible that the HI densities based on DLA data led to underestimations at higher redshifts for GARD. It is also possible that the simulation did not properly account for gas which inflows but is then expelled shortly after, so is not present inside galaxies at later epochs. Finally, the simulated GARD denote the gas accreted onto dark matter halos, whereas we measure gas accretion onto galaxies, as explained in Section 3. Assuming that some gas accretes onto halos, but does not end up inside galaxies, it is not surprising that the simulated GARD is higher than the measured one.

This work could be considerably improved upon by a wider range of data. The lack of H_2 data at higher redshifts might have affected the gas accretion determination. This will be improved by the Atacama Large Millimeter Array (ALMA) and the Northern Extended Millimeter Array (NOEMA) which will perform CO-line scans leading to the determination of ρ_{H_2} (Walter et al. 2014, 2016). On the other hand the Square Kilometre Array (SKA) will deliver direct measurements of ρ_{HI} at least at $z < 1$, which will make it possible to test the result of a constant GARD in this regime.

We do not include the ionized medium in eq. 1 because, even though its filling factor is large (fig. 11 of Kalberla & Kerp 2009), its mass fraction is minor. In the Milky Way by mass the fraction of the ionized ISM ranges from $\sim 2\%$ (from integrating ISM phase profiles in table 5 of Wolfire et al. 2003) to $\sim 23\%$ (table 1.2 of Draine 2011). If this is common among galaxies, then the contribution of the ionized medium to the changes of the total densities we measure is therefore likely smaller than the uncertainties involved.

6 CONCLUSIONS

Star formation rate has not been constant throughout the history of the Universe. This work sought to demonstrate whether the gas accretion onto galaxies over time has affected star formation rate. GARD in this work represents a simply calculated value that shows how much gas mass

density has been accreted by galaxies over a certain redshift interval. If there was a tight correlation between GARD and SFRD then it might suggest that the rate of gas accretion is the limiting factor on SFR. However, a constant GARD, which we measured, might suggest that factors other than the quantity of gas being accreted affect SFRD.

ACKNOWLEDGEMENTS

We thank our referee Jorge Sánchez Almeida for useful comments, and Avery Meiksin, Jochan Fynbo, and Sijing Shen for advise on ISM and DLAs. M.J.M. acknowledges the support of the UK Science and Technology Facilities Council (STFC) and the National Science Centre, Poland through the POLONEZ grant 2015/19/P/ST9/04010. This project has received funding from the European Union's Horizon 2020 research and innovation programme under the Marie Skłodowska-Curie grant agreement No. 665778.

REFERENCES

- Bolatto A. D., Wolfire M., Leroy A. K., 2013, *ARA&A*, 51, 207
 Carilli C. L., Walter F., 2013, *ARA&A*, 51, 105
 Chang T.-C., Pen U.-L., Bandura K., Peterson J.B., 2010, *Nature*, 466, 463
 Cresci G., Mannucci F., Maiolino R., Marconi A., Gnerucci A., Magrini L., 2010, *Nature*, 467, 811
 Decarli R., Walter F., Aravena M., Carilli C., Bouwens R., da Cunha E., Daddi E., Ivison R. J., Popping G., Riechers D., Smail I., Swinbank M., Weiss A., Anguita T., Assef R., Bauer F., Bell E. F., Bertoldi F., Chapman S., Colina L., Cortes P. C., Cox P., Dickinson M., Elbaz D., González-López J., Ibar E., Infante L., Hodge J., Karim A., Le Fevre O., Magnelli B., Neri R., Oesch P., Ota K., Rix H. W., Sargent M., Sheth K., van der Wel A., van der Werf P., Wagg J., 2016, *ApJ*, 833, 69
 Dekel A., Birnboim Y., 2006, *MNRAS*, 368, 2
 Dekel A., Birnboim Y., Engel G., Freundlich J., Goerdt T., Muncuoglu M., Neistein E., Pichon C., Teyssier R., Zinger E., 2009, *Nature*, 457, 451
 Delhaize J., Meyer M. J., Staveley-Smith L., Boyle B. J., 2013, *MNRAS*, 433, 1398
 Draine B. T., 2009, *Cosmic Dust - Near and Far*, ASPCS, 414, 453
 Draine B. T., 2011, *Physics of the Interstellar and Intergalactic Medium*, Princeton University Press
 Fraternali F., 2014, *IAU Symposium*, 298
 Freudling W., Staveley-Smith L., Catinella B., Minchin R., Calabretta M., Momjian E., Zwaan M., Meyer M., O'Neil K., 2011, *ApJ*, 727, 40
 Fynbo J. P. U., Laursen P., Ledoux C., Møller P., Durgapal A. K., Goldoni P., Gullberg B., Kaper L., Maund J., Noterdaeme P., Östlin G., Strandet M. L., Toft S., Vreeswijk P. M., Zafar T., 2010, *MNRAS*, 408, 2128
 Fynbo J. P. U., Ledoux C., Noterdaeme P., Christensen L., Møller P., Durgapal A. K., Goldoni P., Kaper L., Krogager J. K., Laursen P., Maund J., Milvang-Jensen B., Okoshi K., Rasmussen P. K., Thorsen T. J., Toft S., Zafar T., 2011, *MNRAS*, 413, 2481
 Fynbo J. P. U., Geier S. J., Christensen L., Gallazzi A., Krogager J. K., Krühler T., Ledoux C., Maund J. R., Møller P., Noterdaeme P., Rivera-Thorsen T., Vestergaard M., 2013, *MNRAS*, 436, 361
 Hatsukade B., Ohta K., Endo A., Nakanishi K., Tamura Y., Hashimoto T., Kohno K., 2014, *Nature*, 510, 247

Hoppmann L., Staveley-Smith L., Freudling W., Zwaan M. A., Minchin R. F., Calabretta M. R., 2015, MNRAS, 452, 3726

Kalberla P. M. W., Kerp, J., 2009, ARA&A, 47, 27

Kereš D., Yun M.S., Young J.S., 2003, ApJ, 582, 659

Kereš D., Katz N., Weinberg D.H., Davé R., 2005, MNRAS, 363, 2

Krogager J.-K., Fynbo J. P. U., MÅyler P., Ledoux C., Noterdaeme P., Christensen L., Milvang-Jensen B., Sparre M., 2012, MNRAS, 424, L1

Krogager J.-K., Fynbo J. P. U., Ledoux C., Christensen L., Galazzi A., Laursen P., Møller P., Noterdaeme P., PÅlroux C., Pettini M., Vestergaard M., 2013, MNRAS, 433, 3091

L'Huillier B., Combes F., Semelin B., 2012, A&A, 544, A68

Lagos C. D. P., Baugh C. M., Zwaan M. A., Lacey C. G., Gonzalez-Perez V., Power C., Swinbank A. M., van Kampen E., 2014, MNRAS, 440, 920

Lah P. et al., 2007, MNRAS, 376, 1357

Ledoux C., Petitjean P., Fynbo J. P. U., Møller P., Srianand, R., 2005, A&A, 457, 71

Liang C. J., Kravtsov A. V., Agertz O., 2016, MNRAS, 458, 1164

Martin A. M., Papastergis E., Giovanelli R., Haynes M.P., Springob C.M., Stierwalt S., 2010, ApJ, 723, 1359

Martin D. C., Chang D., Matuszewski M., Morrissey P., Rahman S., Moore A., Steidel C. C., 2014, ApJ, 786, 106

Masui K.W., Switzer E.R., Banavar N., Bandura K., Blake C., Calin L.-M., Chang T.-C., Chen X., Li Y.-C., Liao Y.-W., 2013, ApJ, 763, L20

Michałowski M., Hjorth J., Watson D., 2010, A&A, 514, A67

Michałowski et al., 2015, A&A, 582, A78

Michałowski et al., 2016, A&A, 595, A72

Møller P., Fynbo J. P. U., Fall S. M., 2004, A&A, 422, 33

Monier E. M., Turnshek D. A., Rao S., 2009, MNRAS, 397, 943

Noterdaeme P. et al., 2012, A&A, 547, L1

Perley D. A. et al., 2017, MNRAS, 465, L89

Péroux C., McMahon R. G., Storrie-Lombardi L. J., Irwin M. J., 2003, MNRAS, 346, 1103

Péroux C., Dessauges-Zavadsky M., D'Odorico S., Sun Kim T., McMahon R. G., 2005, MNRAS, 363, 479

Prochaska J.X., Wolfe A.M., 2009, ApJ, 696, 1543

Rao S.M., Turnshek D.A., Nestor D.B., 2006, ApJ, 636, 610

Rao S. M., Belfort-Mihalyi M., Turnshek D. A., Monier E. M., Nestor D. B., Quider A., 2011, MNRAS, 416, 1215

Rauch M., Becker G. D., Hahnelt M. G., 2016, MNRAS, 455, 3991

Rhee J., Zwaan M.A., Briggs F.H., Chengalur J.N., Lah P., Oosterloo T., Van Der Hulst T., 2013, MNRAS, 435, 2693

Rhee J., Lah P., Chengalur J.N., Briggs F.H., Colless M., 2016, MNRAS, 460, 2675

Sánchez-Almeida J., Muñoz-Tuñón C., Elmegreen D. M., Elmegreen B. G., Méndez-Abreu J., 2013, ApJ, 767, 74

Sánchez-Almeida J., Elmegreen B.G., Muñoz-Tuñón C., Elmegreen D.M., 2014, A&A Rev., 22, 71

Sancisi R., Fraternali F., Oosterloo T., van der Hulst T., 2008, A&A Rev., 15, A189

Schaye J., Dalla Vecchia C., Booth C. M., Wiersma R. P. C., Theuns T., Haas M.R., Bertone S., Duffy A. R., McCarthy I. G., van de Voort F., 2010, MNRAS, 402, 1536

Stanway E. R., Levan A. J., Tanvir N. R., Wiersema K., van der Laan T. P. R., 2015, ApJ, 798, L7

Turner J. L., Beck S. C., Benford D. J., Consiglio S. M., Ho P. T. P., Kovács A., Meier D. S., Zhao J.-H., 2015, Nature, 519, 331

Walter F., Decarli R., Sargent M., Carilli C., Dickinson M., Riechers D., Ellis R., Stark D., Weiner B., Aravena M., Bell E., Bertoldi F., Cox P., Da Cunha E., Daddi E., Downes D., Lentati L., Maiolino R., Menten K. M., Neri R., Rix H.-W., Weiss A., 2014, ApJ, 782, 79

Walter F., Decarli R., Aravena M., Carilli C., Bouwens R., da

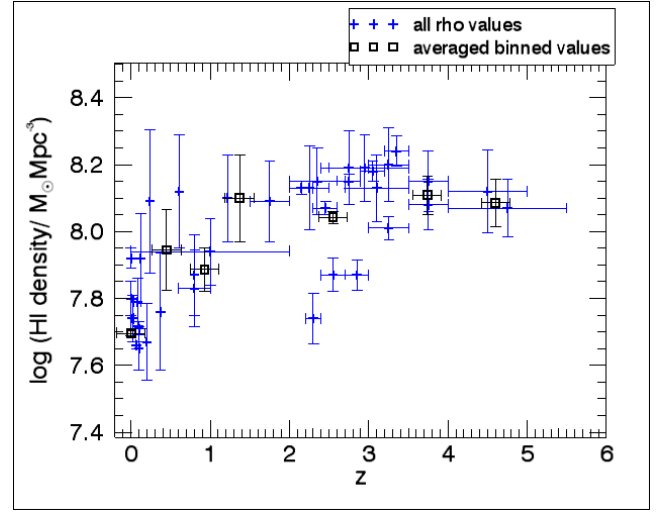


Figure A1. Atomic gas density ρ_{HI} (blue crosses) vs redshift, and the average ρ_{HI} for each redshift bin (black squares).

Cunha E., Daddi E., Ivison R. J., Riechers D., Smail I., Swinbank M., Weiss A., Anguita T., Assef R., Bacon R., Bauer F., Bell E. F., Bertoldi F., Chapman S., Colina L., Cortes P. C., Cox P., Dickinson M., Elbaz D., González-López J., Ibar E., Inami H., Infante L., Hodge J., Karim A., Le Fevre O., Magnelli B., Neri R., Oesch P., Ota K., Popping G., Rix H. W., Sargent M., Sheth K., van der Wel A., van der Werf P., Wagg J., 2016, ApJ, 833, 67

Wolfe A. M., Gawiser E., Prochaska J. X., 2005, ARA&A, 43, 861

Wolfire M. G.; McKee, Christopher F., Hollenbach, D., Tielens, A. G. G. M., 2003, ApJ, 587, 278

Zafar T., Péroux C., Popping A., Milliard B., Deharveng J.M., Frank S., 2013, A&A, 556, A141

Zwaan M. A., Meyer M. J., Staveley-Smith L., Webster R. L., 2005, MNRAS, 359, 30

APPENDIX A: FURTHER PLOTS

We plot here the complete data sets for ρ_{HI} and ρ_{stel} , overplotted with the binned data. The ρ_{HI} data followed an increasing trend from $z = 0$ to 1.5, after which it seems to remain constant.

APPENDIX B: ρ_{HI} DATA COMPILATION

The ρ_{H_2} data came from Kereš et al. (2003) and Decarli et al. (2016). The full ρ_{stel} compilation was sourced from Michałowski et al. (2010). Our complete ρ_{HI} compilation is presented in full in table B1.

This paper has been typeset from a $\text{\TeX}/\text{\LaTeX}$ file prepared by the author.

Table B1. Compilation of atomic gas mass densities, ρ_{HI} . DLA indicates damped Lyman- α .

z	z width	$\log \rho_{HI}$ [$M_{\odot}Mpc^{-3}$]	lower error $\log \rho_{HI}$ [$M_{\odot}Mpc^{-3}$]	upper error $\log \rho_{HI}$ [$M_{\odot}Mpc^{-3}$]	Type of ρ_{HI} measurement	Reference
0.0	0.0	7.80	0.05	0.05	HI	Zwaan et al. (2005)
0.0	0.0	7.92	0.03	0.03	HI	Martin et al. (2010)
0.125	0.0	7.92	0.15	0.12	HI	Freudling et al. (2011)
0.065	0.0	7.66	0.01	0.01	HI	Hoppmann et al. (2015)
0.1	0.1	7.71	0.02	0.02	HI	Hoppmann et al. (2015)
0.24	0.0	8.09	0.27	0.16	HI stacking	Lah et al. (2007)
0.02	0.02	7.74	0.10	0.04	HI stacking	Delhaize et al. (2013)
0.085	0.045	7.79	0.09	0.05	HI stacking	Delhaize et al. (2013)
0.1	0.0	7.65	0.07	0.06	HI stacking	Rhee et al. (2013)
0.2	0.0	7.67	0.13	0.10	HI stacking	Rhee et al. (2013)
0.37	0.0	7.76	0.21	0.14	HI stacking	Rhee et al. (2016)
0.8	0.0	7.87	0.14	0.10	HI intensity mapping	Chang et al. (2010)
0.8	0.2	7.83	0.13	0.10	HI intensity mapping	Masui et al. (2013)
1.0	1.0	7.94	0.10	0.10	DLA	Péroux et al. (2003)
2.35	0.35	8.15	0.10	0.10	DLA	Péroux et al. (2003)
3.1	0.4	8.13	0.10	0.10	DLA	Péroux et al. (2003)
2.95	0.55	8.19	0.10	0.10	DLA	Péroux et al. (2003)
0.609	0.0	8.12	0.20	0.14	DLA	Rao et al. (2006)
1.219	0.0	8.10	0.15	0.11	DLA	Rao et al. (2006)
2.15	0.15	8.13	0.02	0.02	DLA	Noterdaeme et al. (2012)
2.45	0.15	8.07	0.02	0.02	DLA	Noterdaeme et al. (2012)
2.75	0.15	8.15	0.02	0.02	DLA	Noterdaeme et al. (2012)
3.05	0.15	8.18	0.03	0.03	DLA	Noterdaeme et al. (2012)
3.35	0.15	8.24	0.05	0.04	DLA	Noterdaeme et al. (2012)
1.75	0.25	8.09	0.14	0.10	DLA	Zafar et al. (2013)
2.25	0.25	8.13	0.14	0.11	DLA	Zafar et al. (2013)
2.75	0.25	8.19	0.12	0.10	DLA	Zafar et al. (2013)
3.25	0.25	8.20	0.12	0.10	DLA	Zafar et al. (2013)
3.75	0.25	8.15	0.10	0.08	DLA	Zafar et al. (2013)
4.5	0.5	8.12	0.14	0.11	DLA	Zafar et al. (2013)
2.3	0.1	7.74	0.08	0.07	DLA	Prochaska & Wolfe (2009)
2.55	0.15	7.87	0.05	0.05	DLA	Prochaska & Wolfe (2009)
2.85	0.15	7.87	0.05	0.04	DLA	Prochaska & Wolfe (2009)
3.25	0.25	8.01	0.04	0.03	DLA	Prochaska & Wolfe (2009)
3.75	0.25	8.08	0.08	0.07	DLA	Prochaska & Wolfe (2009)
4.75	0.75	8.07	0.09	0.08	DLA	Prochaska & Wolfe (2009)

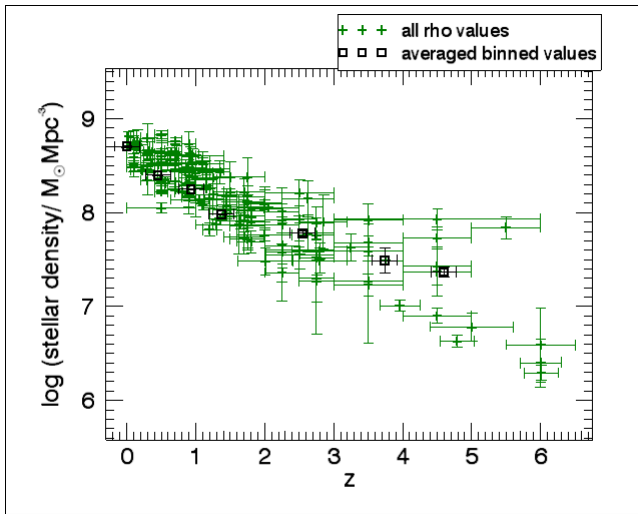


Figure A2. Stellar mass density ρ_{stel} (green crosses) vs redshift, and the average ρ_{stel} for each redshift bin (black squares).

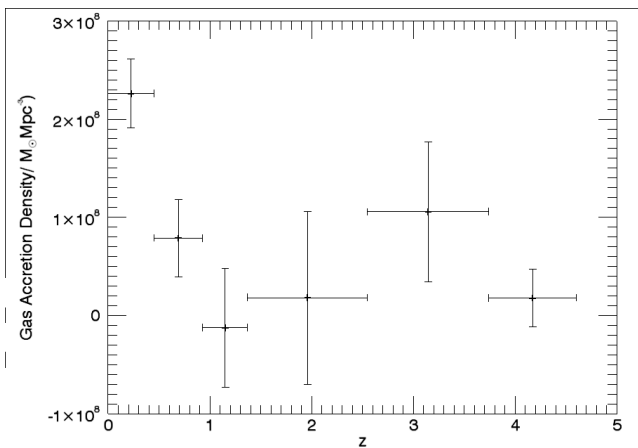


Figure A3. Gas Accretion Density (GAD) against redshift, z . Due to a slight increase in ρ_{tot} between the bins centred at $z = 1.37$ and 0.93 in an otherwise downward trend (see Table 1) the GAD value spanning these bins is negative.